CORE
Metadata, citation and similar papers at core.ac.uk
Provided by Brunel University Research Archive

R134A FLOW PATTERNS IN SMALL DIAMETER TUBES

L. Chen[1] Y. S. Tian[2] and T. G. Karayiannis[1]*

1. Department of Engineering Systems, London South Bank University, 103 Borough Road, London SE1 0AA, U.K.
   Tel: +44 (0) 207 8157628, Fax: +44(0) 207 8157699, E-mail: tassos.karayiannis@lsbu.ac.uk
2. Aspentech Inc., The Gemini Building, Fermi Avenue, Harwell International Business Centre, Didcot, Oxfordshire, OX11 9QR, U.K.
   Tel: +44 (0) 1235 448260, Fax: +44(0) 1235 448230, E-mail: william.tian@aspentech.com

ABSTRACT

R134a vapour-liquid two-phase flow patterns were studied in vertical small diameter tubes. The observed flow patterns include bubbly, dispersed bubble, slug, churn, annular and mist flow. Six integrated flow pattern maps, derived for two internal diameters (2.01 and 4.26 mm) and three different pressures (6.0, 10.0, 14.0 bar), are presented. Some transition boundaries, such as slug-churn and churn-annular, were found to be very sensitive to diameter and pressure. On the contrary, the boundaries of dispersed bubble-churn and bubbly-slug are less affected. The transition boundaries are compared with the existing models for normal size tubes showing significant differences.

Keywords: two-phase flow, flow patterns, small diameter, vertical flow, pressure.

INTRODUCTION

Small and micro heat transfer devices are used with increasing frequency in the fields of energy, chemical and petroleum industries and in domestic appliances and computers. Typical applications include compact heat exchangers in air-conditioning and refrigeration systems, thermal control devices in spacecrafts, chemical processing systems, high power electronic device cooling systems et al. [1-3]. However, up to now, the study of two-phase flow regimes in small channels is still at an early stage though there is a significant number of reports in this field. The present authors examined the previous studies for small tubes and channels and concluded that the majority of them dealt with adiabatic air-water in rectangular channels with a hydraulic diameter range of 1 to 5 mm and flow flux range of 1 to 1x10^4 kg/m^{2}s. Although researchers agreed that surface tension becomes an important parameter with the decrease of the channel dimension [1, 4-6], the flow pattern transition mechanisms for small channels are quite vague and disputable. It is still therefore, problematic or impossible to predict the flow patterns for small channels due to lack of adequate experiment data and theoretical analysis.

In addition, the existing limited experimental data revealed large discrepancies among different investigators. For example, the definition of small tube has not been generally agreed. Some particular flow patterns reported by Oya [4], such as granular-lumpy bubble and fish-scale type slug flows were not observed in other experiments. The flow maps sketched by different researchers may be dissimilar even though they use similar tubes under similar conditions. For instance, the vertical upward flow maps by Fukano and Kariyasaki [1], Oya [4], Barnea et al. [5], Mishima and Hibiki [7] are not in agreement. The horizontal flow maps by Fukano and Kariyasaki [1], Barnea et al. [5], Damianides and Westwater [8], Coleman and Garimella [9], Triplett et al. [10 also show differences. Some researchers thought that the existing models or empirical maps for normal size tubes could predict flow patterns well in small tubes except some transition boundaries. For example, Mishima and Hibiki [7] carried out experiments and sketched air-water flow maps for 1 to 4 mm vertical tubes. They found that the transition boundaries were predicted well by the Mishima-Ishii's model [11]. Barnea et al. [5] compared the experimental data of 4-12 mm vertical and horizontal tubes with the physical models for normal tubes presented in Taitel and Dulkler [12] and Taitel et al. [13]. They reported satisfactory comparisons except for the stratified-intermittent flow transition boundary in horizontal flow. On the contrary, most researchers found that two-phase flow patterns in small tubes could not be properly predicted by the existing correlations developed for normal tubes [1, 9 and 10].

Other ambiguities involve the effect of controlling parameters on flow pattern transition boundaries, which is very important in establishing reasonable correlations. The following parameters can affect flow patterns, see Taitel [16]:

(1) Liquid and gas superficial velocity, U_{ls} and U_{gs}
(2) liquid and gas density, ρ_l and ρ_g
(3) liquid and gas dynamic viscosity, μ_l and μ_g
(4) diameter, d
(5) gravitational acceleration g and tube inclination θ
(6) surface tension, σ
(7) tube roughness, ε

*: Corresponding author

Taitel suggested that the above eleven dimensional parameters can be reduced to eight dimensionless parameters. In addition, flow boiling should include heat flux (q) and enthalpy h_g, h_l or h_{fg}. Although the above thirteen parameters can be simplified to eight parameters in vertical adiabatic two-phase flow in a smooth tube, i.e. U_{ls}, U_{gs}, ρ_l, ρ_g, μ_l, μ_g, d, σ, it is still quite impractical to find a relation for them based on experimental data or theoretical analysis. Clearly, density, viscosity and surface tension are not independent parameters in liquid-vapour flow and they are a function of the saturated pressure. The most important controlling parameters can be further reduced to superficial velocities, diameter and pressure. However, the deduced correlations would then apply to the tested fluids only, i.e. will not be universally applicable.

The effect of pressure upon flow patterns has been investigated by several experimentalists using different fluids. McQuillan and Whalley [14] compared the water-steam flow pattern maps in a 10 mm vertical tube at different pressures and found that the slug-churn and churn-annular boundaries shift slightly towards the region of low vapour flow rate when the pressure increases.

Theoretically, flow patterns are less affected by channel orientation in small channels since the relative effect of gravity is smaller than in large tubes. Therefore, the effect of channel dimension on the transition boundaries should be similar whether in vertical or in horizontal flow. However, researchers hardly reached agreement on this area, as shown in Table 1.

Table 1. The direction of boundary shift with reducing channel dimensions

Researcher	dimension and orientation	dispersed bubble to intermittent [1]	slug to churn	to annular
Damianides & Westwater [8]	1-5 mm, horizontal	Lower U_{ls}		Higher U_{gs}
Lin et al. [6]	0.5-4 mm, vertical		Lower U_{gs}	Lower U_{gs}
Coleman & Garimella [9]	1.3-5.5 mm horizontal	Higher U_{ls}		Higher U_{gs}

1. Intermittent flow: plug or slug for horizontal tube and bubbly or slug for vertical tube.

Despite the above discrepancies, some common characteristics exhibited in small tubes have been recognized by various researchers [1, 4, 7, 8, 10 and 15]:

(1) Higher heat transfer capability.
(2) Surface tension is a predominant force.
(3) Flow patterns are less affected by channel orientation.
(4) Flow patterns are mostly axisymmetric in horizontal or inclined tubes.
(5) Bubbles tend to be regular in shape, i.e. round.
(6) Some special flow patterns emerge (not reported in large size tubes).
(7) Intermittent flow appears easily and the stratified flow is suppressed.
(8) The confined bubble flow becomes a typical regime in horizontal flow.
(9) There is a thinner liquid film around the plug bubbles.
(10) There is a lower bubble free lift velocity in vertical flow.

In the work described in this paper, we carried out detailed and accurate flow visualization experiments on adiabatic flow patterns in small tubes using R134a in order to (i) obtain flow pattern maps, (ii) compare these with the existing models, (iii) verify the effect of pressure and (iv) the effect of diameter on flow patterns and transition boundaries.

EXPERIMENTAL FACILITY

The designed experimental facility is capable of covering a wide range of all typical flow patterns, which include bubbly, dispersed bubble, slug, churn, annular and mist flow. The entire facility can be divided in three parts, i.e. the R22 cooling system, the R134a experimental system and the control and data acquisition system. The R134a loop is composed of (a) a tank (b) a circulating pump (c) two Coriolis mass flow meters (d) a chiller (e) a preheater (f) a test section (g) a separator and (h) a condenser, see Figure 1. This figure does not include the R22 cooling system and the control and data acquisition system. The R22 cooling system is used to cool and condense R134a at the chiller and condensers respectively. Most of the refrigerant 134a in the system is stored in the tank, in which a heater is installed to control the system pressure. The pump circulates the liquid refrigerant to the flow meters, the chiller and then the preheaters, where the refrigerant is controlled to the desired degree of subcooling at the inlet of the test section. Two test sections with internal diameters 2.01 and 4.26 mm were examined. The test section shown schematically in Figure 2, can be subdivided into three parts; namely the calming section, the heating section and the observation section. Single-phase liquid passes through the calming section, which ensures full-developed flow. Two-phase flow is created by supplying high electric current directly onto the steal tube – the heating section. The observation section, a Pyrex glass tube, is directly connected to and has the same inner diameter as the steel heating tube. Flow patterns were observed and recorded by a high-speed camera (Phantom V4 B/W, 512x512 pixels resolution, 1000 pictures/second with full resolution and maximum 32000 pictures/second with reduced resolution, 10 microseconds exposure time). After the test section, the two-phase refrigerant is separated into liquid and vapour in the separator; the liquid flows back to the tank directly while the vapour is first condensed. The flow rate is controlled by three control valves located in the main loop and bypass. The control and data acquisition system enables the automatization of the data collection and the parametric control, reduces manual operation and improves measuring precision. The measured parameters include flow rate (F1 or F2), power (DPM2) and pressure and temperature at the test section (P3, T3, P4, T4, P0, T0). The thermocouples T3, T4, and T0 use the water freezing point as reference to improve the measuring accuracy. The energy loss at the test section is calculated based on the temperature difference at the inner-outer insulation surface surrounding the test section and a thermal loss coefficient. The thermal loss coefficient was estimated based on single-phase experiments. The signals from P0, T7 are exported to a PID controller. The P0 signal is used to automatically adjust the system pressure through controlling the heater in the refrigerant tank. The T7 signal controls the variable heater of the preheater so as to achieve the desired subcooling degree at the inlet of the test section.

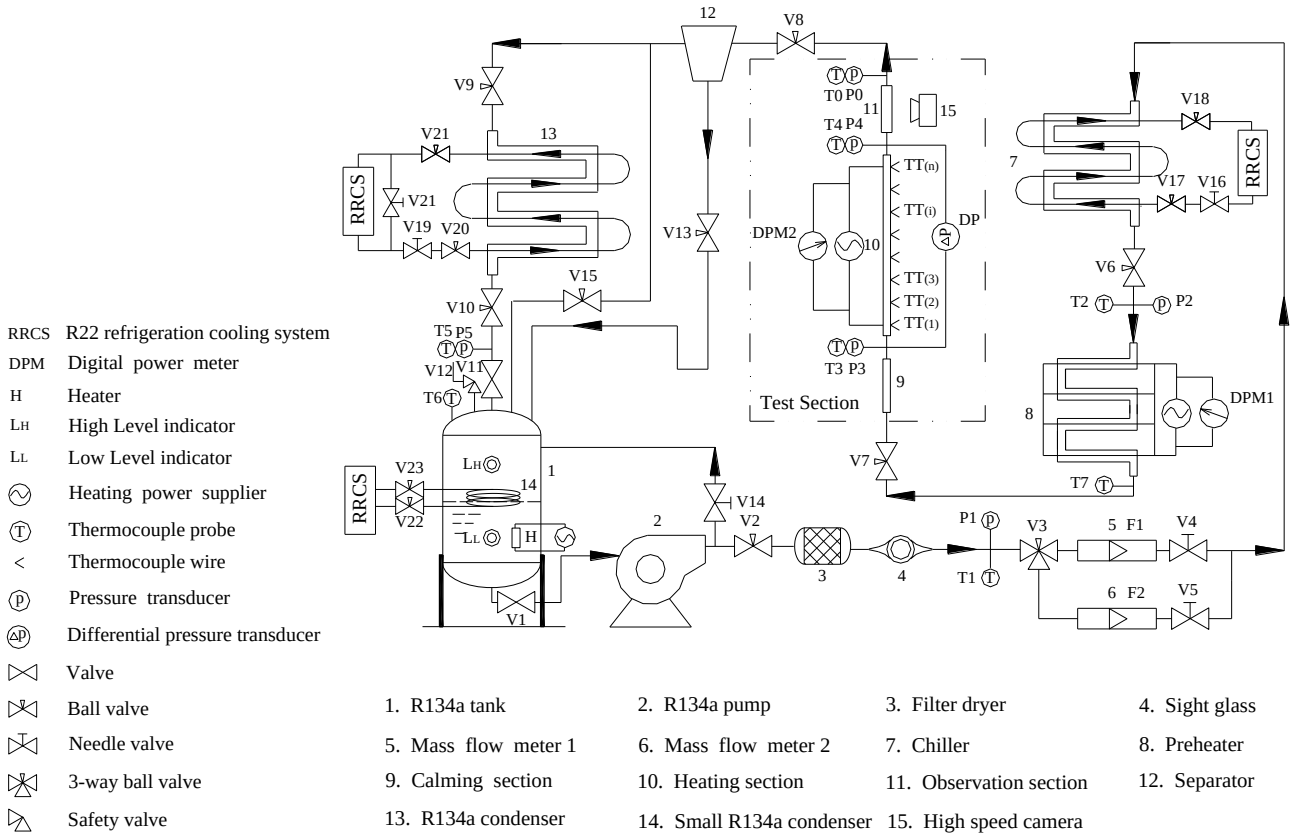

Figure 1. Schematic diagram of the flow patterns experimental facility (the R22 plant is not shown).

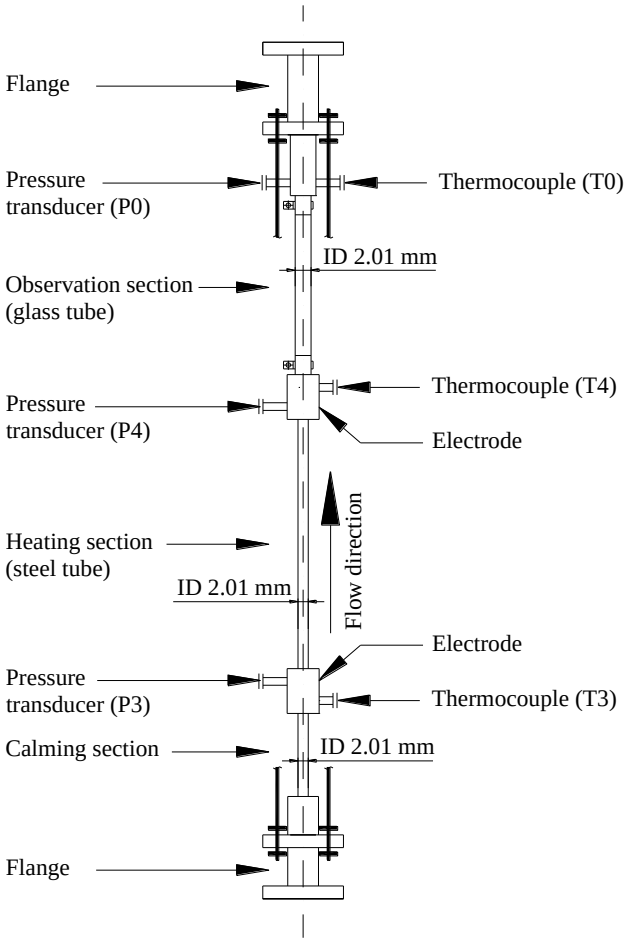

Figure 2. Schematic diagram of the test section (2.01 mm tube).

All the instruments were carefully calibrated. The measuring uncertainty in temperature is ± 0.2 K, pressure ± 0.15 %, flow rate ± 0.4 %, and power ± 0.6 %. The overall system performance was validated through single-phase experiments. Turbulent experimental friction factor agreed with the Blasius equation within ± 5 % over the Reynolds range of 4000 to 110000. The experimental parameters in the two-phase flow patterns experiments were deduced from the inlet and outlet saturated pressure and the assumption that the pressure drop along the observation section was linear. The liquid and vapour superficial velocities were varied and calculated for each diameter and pressure by changing the flow rate and heating power. During the experiments, the liquid superficial velocity was held at a constant value first while the vapour superficial velocity was increased gradually until annular flow emerged. The number of data points obtained at the transition boundaries was higher than at other conditions. The local superficial velocities at the observation point were calculated as follows:

$$U_{gs} = \frac{\dot{m}\, x}{A\rho_g} \tag{1}$$

$$U_{ls} = \frac{\dot{m}(1-x)}{A\rho_l} \tag{2}$$

where,

$$x = \frac{\dot{m}(h_{in} - h_l) + (Q - \Delta Q)}{\dot{m}(h_g - h_l)} \tag{3}$$

Here, mass flow rate ($\dot{m}$) and power (Q) were measured by the Coriolis mass flow meters (F1 or F2) and the power meter (DPM2) respectively. The inlet enthalpy (h_{in}) was calculated based on the temperature and pressure at the inlet of the heating section (T3, P3) and the saturated parameters at the observation point (ρ_g, ρ_l, h_g, h_l) were calculated based on the local saturated pressure, which was deduced from the pressure at the inlet and outlet of the observation section (P4, P0) – the pressure drop was assumed linear. Also, as stated earlier, the thermal loss at the test section (ΔQ) was obtained using the temperature difference (ΔT) across the insulation and the thermal loss coefficient (K). In these case, K is 0.116 and 0.086 W/K for the 4.26 mm and 2.01 mm test section respectively.

The collected data are the key parameters that affect flow patterns: two tube diameters d, mass flow rate m, input power Q, pressure P and the corresponding saturated temperature T were tested and recorded during the experiments. Other parameters, such as quality (x), liquid and vapour superficial velocities (U_{ls}, U_{gs}), liquid and vapour densities (ρ_l, ρ_g), liquid and vapour viscosity (μ_l, μ_g), surface tension σ, were deduced from these data and from the mass and energy conversation equations as shown above. The range of the experiments is given in Table 2. The R134a parameters in the range of the experimental pressure of the current tests are listed in Table 3.

Table 2. The range of the current experiments.

Parameters	Range	Unit
Diameter	2.01, 4.26	mm
Pressure	0.6, 1.0, 1.4	MPa
Superficial vapour velocity	0.01- 16.9	m/s
Superficial liquid velocity	0.04 – 5.55	m/s

Table 3. R134a thermophysical data for the range of pressure studied.

Parameters	Value			Unit
Pressure	0.6	1.0	1.4	MPa
Temperature	21.6	39.4	52.5	°C
Vapour Density	29.0	49.1	70.7	kg/m^3
Liquid Density	1218	1148	1090	kg/m^3
Vapour Dynamic Viscosity	0.0117	0.0126	0.0133	Pa s
Liquid Dynamic Viscosity	0.210	0.171	0.147	Pa s
Surface Tension	0.0084	0.0062	0.0046	N/m

EXPERIMENTAL RESULTS

The accurate identification of flow patterns and transition boundaries is quite difficult due to lack of agreement on classification and the subjectivity of observers. Some researchers like to use very detailed classifications; others prefer less detailed divisions because extremely detailed classifications are insignificant in engineering. Taitel [16] wrote that the trend was to report the number of flow patterns to the minimum essential with the desire to reach standardization so that data from different laboratories could be correctly interpreted and compared. Currently, most researchers agree to categorize their observations into four main flow patterns: stratified flow, intermittent flow, annular flow and bubble flow. Each main class could be subdivided into subclasses. For example, Taitel [16] and Barnea [17] defined five typical flow patterns in their vertical upward flow pattern maps, i.e. dispersed bubble, bubbly, slug, churn and annular. We follow the above categorization in our study. Occasionally mist flow was observed at very high vapour velocity. The above-mentioned six flow patterns are defined as follows:

Dispersed bubble: numerous small bubbles float in a continuous liquid phase.

Bubbly: bubble size is comparable to but not as large as the tube diameter.

Slug: bubbles develop into bullet shape due to the tube wall restriction. Sometimes the bullet bubbles are followed by a stream of small bubbles creating a trail.

Churn: bullet bubbles start to distort and small bubbles in liquid slug coalesce into gas clump with increase of gas velocity. It is a highly oscillatory flow with chaotic interface.

Annular: gas phase becomes a continuous flow in the core of the tube.

Mist: liquid film is blown away from tube wall and numerous liquid droplets float in high-speed vapour flow.

Figures 3 and 4 show the above flow patterns obtained by the digital high-speed camera in the 2.01 and 4.26 mm diameter tubes at 10 bar pressure. The flow patterns in the two tubes are similar and could be grouped into the above six typical patterns – note that no mist flow was obtained in the 2.01 mm tube since critical heat flux was reach. Similar results were obtained at system pressure 6 and 14 bar. All the flow patterns for both tubes observed in the experiments were of the typical categories mentioned above. However, on closer observations, there are some differences in these two tubes. The flow patterns in the 4.26 mm tube do not exhibit any common characteristics of the flow patterns in small tubes; i.e. the irregular bubbles, the shorter plug, the thicker liquid film around the plug, and the chaotic vapour-liquid interface in churn flow. This means that the surface tension of R134a is still a weak force at 4.26 mm and this diameter is not small enough to confine the flow. This indicates that as far as flow patterns are concerned, the 4.26 mm tube behaves like a traditional tube when using refrigerant R134a as fluid. Comparatively, the flow patterns in the 2.01 mm tube showed some “small tube characteristics”, which indicate the increasing action of the surface tension and the tube confinement, e.g. the slimmer plug, the thinner liquid film around the plug, and the less chaotic vapour-liquid interface in churn flow. Therefore, the 2.01 mm tube possesses both characteristics of the normal size and the small tube. Thus 2 mm could be regarded as a critical diameter for refrigerant R134a for the current range of experimental conditions. This will be examined further in future experiments which will include smaller inner diameter tubes.

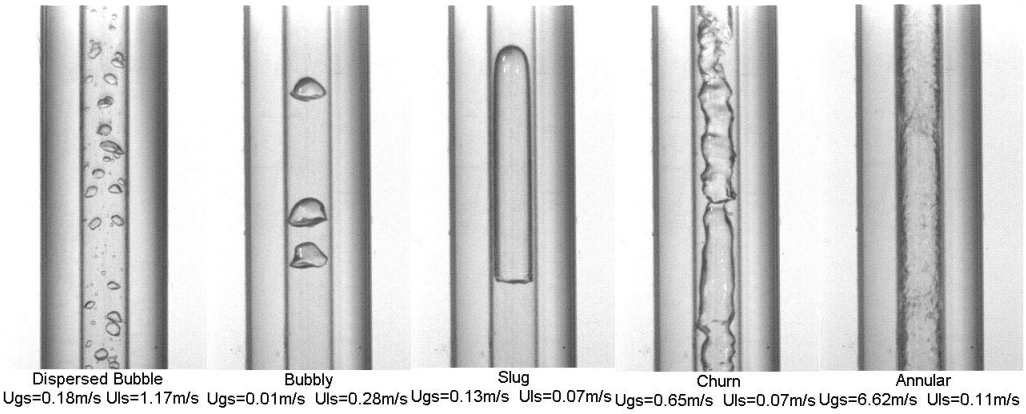

Figure 3. Flow patterns observed in the 2.01 mm internal diameter tube at 10 bar.

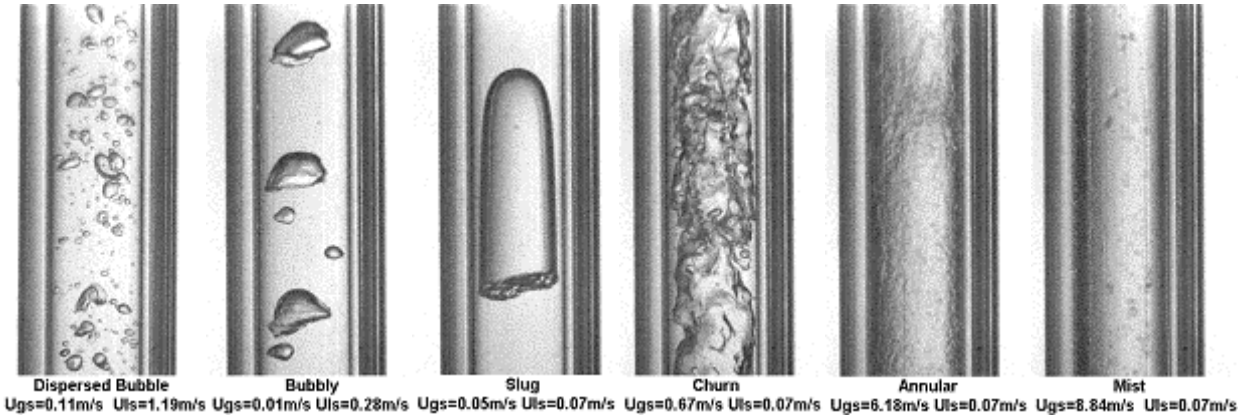

Figure 4. Flow patterns observed in the 4.26 mm internal diameter tube at 10 bar.

Six flow pattern maps were generated based on all the observed results for the 2.01 and 4.26 mm tubes at 6, 10 and 14 bar pressure. The flow pattern map for the 4.26 mm tube at 10 bar is presented first and compared with the existing models for vertical upward flow in normal size tubes. They are the unified model summarized by Taitel [16] and the models given by Taitel [13], Mishima and Ishii [11] and McQuilian and Whalley [14]. The comparisons are presented in Figures 5-8, where the solid lines plotted were based on the equations provided by the above authors. Although the flow patterns for R134a in the 4.26 mm tube exhibit strong characteristics of the normal size tube, the agreement between the maps and the models is still very poor. The unified model predicts the transition boundary of dispersed bubble to slug (including bubbly) flow fairly well but it creates a region where the churn-annular boundary falls in the slug flow zone rather than on the right side (higher U_{gs}) of the slug - churn boundary. The dispersed bubble – bubbly boundary shown in Figure 6 indicates an increase in U_{ls} with U_{gs}. Taitel [13] grouped bubbly flow in with slug flow and noted that the boundary between dispersed bubble to slug flow show a decrease U_{ls} with increases in U_{gs}. In addition, Mishima and Ishii's model (Figure 7) predicts an extremely small churn zone whereas in our experiments churn is a main flow pattern. The model proposed by McQuilian and Whalley [14] is in complete disagreement with our experimental results, see Figure 8. The above models had been validated in previous experiments but most of them used air – water. Therefore, it is difficult to determine which is the main factor, which causes the discrepancies – diameter or fluid. The comparison of the present results for the smaller 2.01 mm internal diameter tube with the model summarized by Taitel [16] is depicted in Figure 9. We chose to present the comparison with this model since it appears from the examination of Figures 5-8 above to match the experimental observations for the 4.26 mm tube better than the other models. As seen in the figure, the model can no longer predict any of the transition boundaries obtained in our experiments. This indicates that, compared to the 4.26 mm tube, the flow patterns and in particular the transition boundaries, in the smaller tube have started to deviate further from the ones obtained in traditional size tubes.

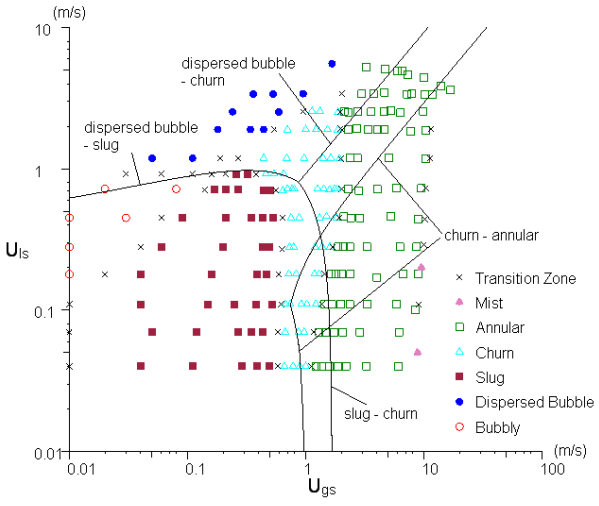

Figure 5. Flow pattern map for R134a in the 4.26 mm tube at 10 bar and comparison with the unified model summarized by Taitel, [16].

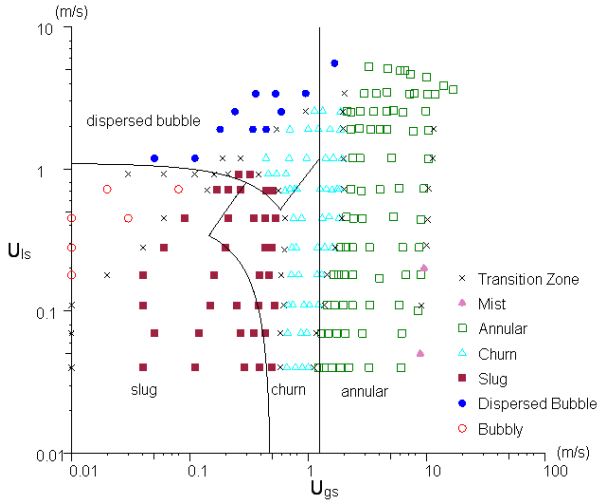

Figure 6. Flow pattern map for R134a in the 4.26 mm tube at 10 bar and comparison with the model of Taitel et al., [13].

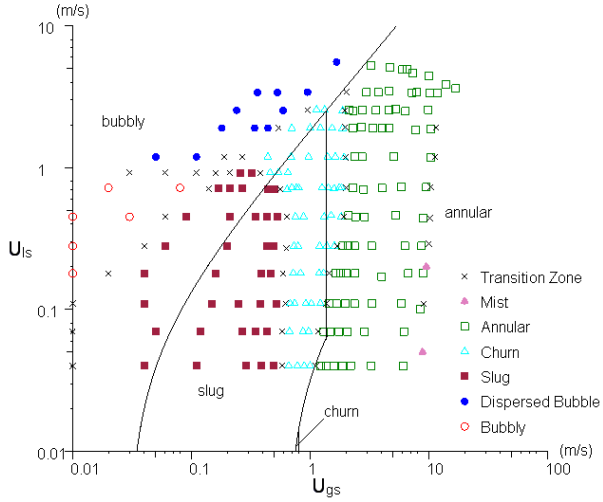

Figure 7. Flow pattern map for R134a in the 4.26 mm tube at 10 bar and comparison with the model of Mishima and Ishii, [11].

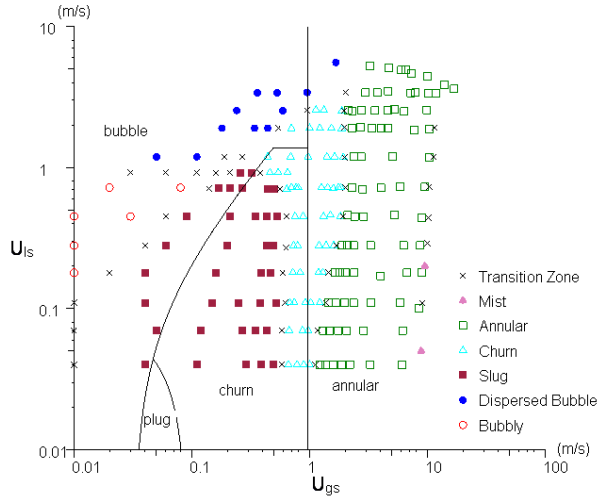

Figure 8. Flow pattern map for R134a in the 4.26 mm tube at 10 bar and comparison with the model of McQuilian and Whalley, [14].

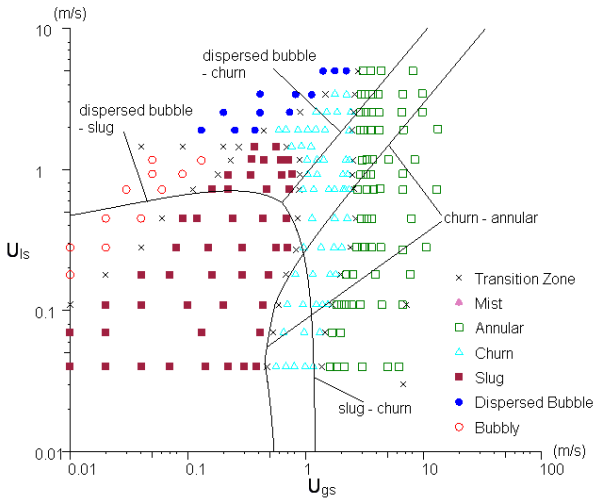

Figure 9. Flow pattern map for R134a in the 2.01 mm tube at 10 bar and comparison with the unified model summarized by Taitel, [16].

The effect of pressure on flow patterns is shown in Figures 10 and 11. Our experimental results lead to the same conclusion as McQuillan and Whalley [14], i.e. the transition boundaries of slug-churn and churn-annular flow shift slightly towards the region of lower vapour flow rate when pressure increases. In addition, the dispersed bubble-bubbly boundary shifts to lower liquid velocity with a pressure increase. The boundaries of dispersed bubble-churn and bubbly-slug are hardly affected by pressure in the current experiments. As shown in Table 3, the surface tension decreases as pressure increases, which may lead to easier (lower U_{gs}) transition of bubbly to dispersed bubble and slug to churn. Also, the value of the vapour density increases significantly when pressure rises; the heavier vapour density increases the vapour momentum at the same vapour velocity and this could result in the transition of churn to annular flow at lower vapour velocity.

The effect of diameter on flow patterns is depicted in Figures 12-14. As seen in the figures, reducing the diameter shifts the transition boundaries of slug-churn and churn-annular to higher values of vapour velocity. This result is in agreement with the experiments of Daminides and Westwater [8] and Coleman and Garimella [9] but contrary to the results of Lin et al. [6], see Table 1. Also, the dispersed bubble-bubbly boundary shifts to higher liquid velocity with a reduction in the diameter; Coleman and Garimella [9] reported the same conclusion for a horizontal tube. However, Damianides and Westwater [8], also for horizontal flow, reported that the intermittent – dispersed bubble boundary moves to the region of lower liquid flow rate with decreasing tube diameter. There seems to be no change for these two diameters at the boundary between dispersed bubble – churn and bubbly-slug flow. The above conclusions will be verified for smaller diameter tubes.

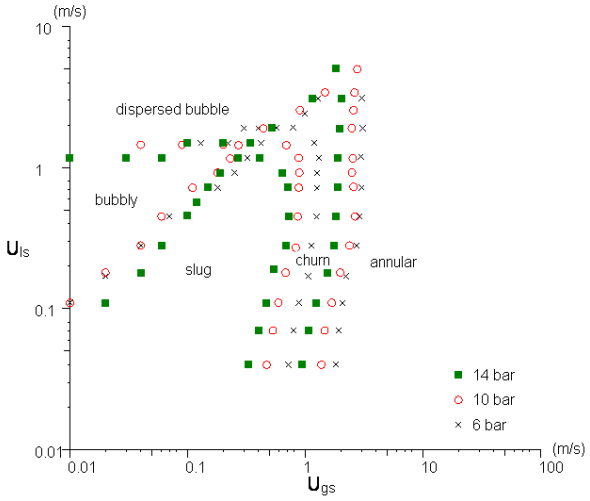

Figure 10. Effect of pressure on transition boundaries with the 2.01 mm tube

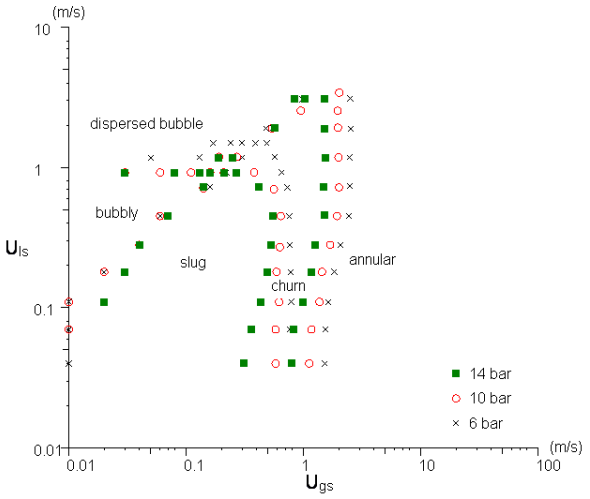

Figure 11. Effect of pressure on transition boundaries with the 4.26 mm tube

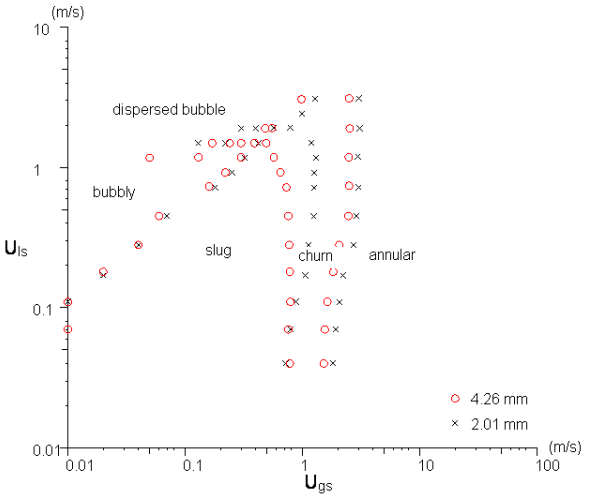

Figure 12. Effect of diameter on transition boundaries at 6 bar

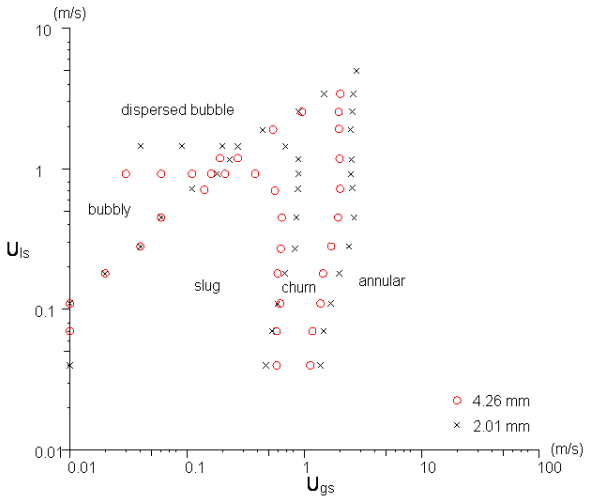

Figure 13. Effect of diameter on transition boundaries at 10 bar

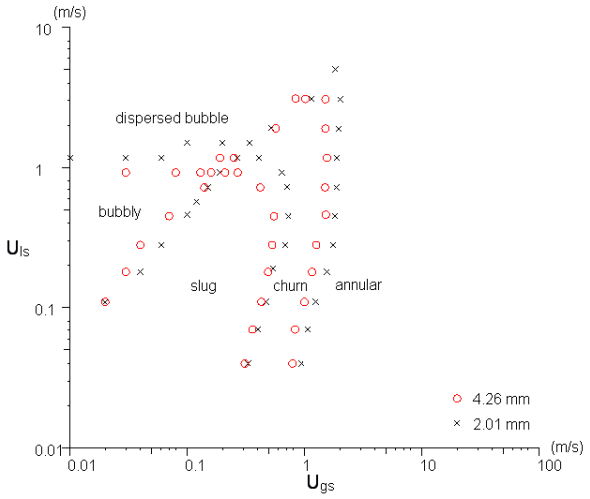

Figure 14. Effect of diameter on transition boundaries at 14 bar

CONCLUSIONS

Six typical flow patterns were observed at the present experimental conditions, i.e. dispersed bubble, bubbly, slug, churn, annular and mist. The experimental results demonstrate that the flow patterns for the larger diameter (4.26 mm) studied are similar to what is expected in traditional size tubes. This also indicates a weak surface tension effect. The reduction of the diameter to 2.01 mm produced a significant effect on the transition boundaries indicating confinement effects and an increasing importance of surface tension. Six flow pattern maps were drawn and compared with the existing models for normal size tubes indicating significant differences at the transition boundaries for the 4.26 mm and more so for the 2.01 mm internal diameter tube. The boundaries of slug-churn and churn-annular moved to higher vapour velocity when the diameter change from 4.26 to 2.01 mm; the dispersed bubble-bubbly boundary moved to higher liquid velocity. The effect of pressure reduction appears to be the same on the above boundaries. No or little effect was observed on the dispersed bubble to churn and bubbly to slug boundaries with diameter or pressure changes.

NOMENCLATURE

A	flow area, m^2
d	bubble diameter, m
h	enthalpy, J/kg
K	thermal loss coefficient, W/K
$\dot{m}$	mass flow rate, kg/s
p	pressure, Pa
q	heat flux, W/m^2
t	temperature, °C
ΔT	temperature difference, K
U	velocity, m/s
Q	heat transfer rate to tube (voltage x current), W
ΔQ	thermal loss, W
x	quality
ε	pipe roughness, m
μ	dynamic viscosity, kg/m s
θ	angle of pipe to horizontal, degrees
ρ	density, kg/m^3
σ	surface tension, N/m

Subscripts

fg	latent heat
g	saturated gas/vapour
gs	superficial gas
in	inlet
l	saturated liquid
ls	superficial liquid

REFERENCES

1. T. Fukano and A. Kariyasaki, Characteristics of gas-liquid two-phase flow in a capillary tube, Nuclear Engineering and Design, Vol. 141, pp. 59-68, 1993.
2. D.C. Zietlow and C.O. Pedersen, Flow regime mapping and analysis of R-134a in a small-channel cross-flow condenser, ASHRAE Transactions, Vol. 104, No. 2, pp. 540-547, 1998.
3. S. Wongwises, S. Disawas, J. Kaewon and C. Onurai, Two-phase evaporative heat transfer coefficients of refrigerant HFC-134a under forced flow conditions in a small horizontal tube, Int. Comm. Heat Mass Transfer, Vol. 27, No. 1, pp. 35-48, 2000.
4. T. Oya, Upward liquid Flow in small tube into which air streams (1st Report, Experimental apparatus and flow patterns), Vol. 14, No. 78, pp. 1320-1329, 1971.
5. D. Barnea, Y. Luninski and Y. Taitel, Flow pattern in horizontal and vertical two phase flow in small diameter pipes, The Canadian Journal of Chemical Engineering, Vol. 61, No. 5, pp. 617-620, 1983.
6. S. Lin, P.A. Kew and K. Cornwell, Two-phase flow regimes and heat transfer in small tubes and channels, Heat Transfer1998, Proceedings of 11th IHTC, Vol. 2, August 23-28, Kyongju, Korea, pp. 45-50, 1998.
7. K. Mishima and T. Hibiki, Some characteristics of air-water two-phase flow in small diameter vertical tubes, Int. J. Multiphase flow, Vol. 22, No. 4, pp. 703-712, 1996.
8. D.A. Damianides and J.W. Westwater, Two-phase flow patterns in a compact heat exchanger and in small tubes, Second UK National Conference on Heat Transfer, Volume 11 Sessions 4A-6C, pp. 1257-1268, 1988.
9. J.W. Coleman and S. Garimella, Characterization of two-phase flow patterns in small diameter round and rectangular tubes, International Journal of Heat and Mass Transfer, Vol. 42, pp. 2869-2881, 1999.
10. K.A. Triplett, S.M. Ghiaasiaan, S.I. Abdel-Khalik and D.L. Sadowski, Gas-liquid two-phase flow in microchannels, Part I: Two-phase flow patterns, International Journal of Multiphase Flow, Vol. 25, Elsevier Science Ltd., pp. 377-394, 1999.
11. K. Mishima and M. Ishii, Flow regime transition criteria for upward two-phase flow in vertical tubes, Int. J. Heat Mass Transfer, Vol. 27, No. 5, pp. 723-737, 1984.
12. Y. Taitel and A. E. Dukler, A model for predicting flow regime transitions in horizontal and near-horizontal flow, AIChE, Vol. 22, pp. 47-55, 1976.
13. Y. Taitel, D. Barnea and A. E. Dukler, Modelling flow pattern transitions for steady upward gas-liquid flow in vertical tubes, AIChE, Vol. 26, pp. 345-354, 1980.
14. K. W. McQuillan and P. B. Whalley, Flow patterns in vertical two-phase flow, Int. J. Multiphase Flow, Vol. 11, No. 2, pp. 161-175, 1985.
15. S. Lin, P.A. Kew and K. Cornwell, Characteristics of air/water flow in small tubes, Heat and Technology, Vol. 17, No. 2, pp. 63-70, 1999.
16. Y. Taitel, Flow pattern transition in two phase flow, Keynote lecture, 9th International Heat Transfer Conference, Jerusalem, Israel, 19-24 Aug., pp. 237-254, 1990.
17. D. Barnea, An unified model for predicting flow-pattern transitions for the whole range of pipe inclinations, Int. J. Multiphase Flow, Vol. 13, No. 1, pp. 1-12, 1987.